Localization of phonons in mixed crystals

Qian-Jin Chu and Zhao-Qing Zhang
Institute of Physics, Chinese Academy of Sciences, Beijing, China
(Received 11 September 1987; revised manuscript received 24 March 1988)

The problem of phonon localization in mixed crystals is formulated using the self-consistent localization theory developed by Vollhardt and Wölfle. The coherent-potential approximation (CPA) is used to obtain the phonon density of states and CPA diffusion constant. Three-dimensional harmonic binary systems with random masses but constant isotropic force are studied in detail. With the use of the semielliptical band approximation, the phase diagrams, mean free path, correlation and localization lengths, and diffusion constant are calculated for various mass ratios and concentrations. The limit when the mass of one component is infinite is also studied.

I. INTRODUCTION

Considerable progress has been made in understanding the nature of electronic states in disordered systems in the past decade.[1] For the case of noninteracting electrons, Anderson localization in different dimensions has been under intensive study. It is now believed that mobility edges exist only in systems with dimension greater than two.[1,2] In three dimensions, the localization phase diagrams have been studied numerically for various models.[3–5] As a wave phenomenon in disordered systems, Anderson localization is recognized to be common to both quantum electrons and classical waves. Since the classical waves offer both the potential for more direct observation of localization as well as the possibility of novel localization characteristics distinct from those of electrons, much interest has been focused recently on the study of localization, both theoretically and experimentally, for various kinds of classical waves like elastic,[6] scalar,[7,8] electromagnetic,[9] and spin waves.[10] There is also increasing interest in the study of phonon localization in solids.[11–15] It has been suggested that the existence of a plateau in the thermal conductivity accompanied by excess specific heat in all glasses could be explained by the localization of the acoustic phonon at some critical frequency.[12,15]

In this work, the properties of acoustic-phonon localization are studied for harmonic mixed crystals with random masses but constant isotropic force. The self-consistent theory of Anderson localization developed by Vollhardt and Wölfle[16] (VW) in conjunction with the coherent-potential approximation[17–19] (CPA) is extended to phonon localization. This method has been used to calculate the mobility edge and localization length for tight-binding electron models and has given results which are in excellent agreement with numerical simulation data.[3] Here, numerical calculations are carried out only for the binary fixed crystals. In three dimensions, with the use of the semielliptical band approximation,[17] the phase diagrams, mean free path, correlation and localization lengths, and diffusion constant are calculated for various mass ratios and concentrations. We find that in certain regions of mass ratio and concentration there are three mobility edges in the band. On the boundaries of these regions two mobility edges appear or disappear simultaneously and the corresponding correlation or localization length diverges with a new exponent different from the one at the usual mobility edge. The case when the mass of one component becomes infinite is also studied.

In Sec. II, phonon localization for mixed crystals is formulated in terms of averaged two-phonon Green's function. CPA is used to obtain the phonon density of states (DOS) and CPA diffusion constant. In Sec. III, the self-consistent diagrammatic theory of VW is used to obtain the diffusion constant and mobility edges. With the use of the semielliptical band assumption, analytic formulas for the DOS, the CPA diffusion constant, the mean phonon velocity, the mean free path, the correlation and localization lengths, and the diffusion constant are given in Sec. IV. Section V contains numerical results for the binary systems and discussions.

II. FORMULATION

Consider a d-dimensional hypercubic harmonic mixed crystal with random masses but constant isotropic force between nearest-neighbor sites. The equations of motion for the displacement u_i along any direction of the lattice have the form

$$m_i\ddot{u}_i+2dKu_i-K\sum_l{}' u_l=0\ , \tag{1}$$

where m_i is the mass on site i, K is the force constant, and the summation of l is over the nearest neighbors of i. In order to study the localization effects, one can study the time and space evolution of the energy density caused by the injected disturbance.[6,7] Consider a local disturbance of velocity impulse $-2\pi/m_j$ at site j at time $t=0$. The energy density at any site i and time t is proportional to $m_i[\dot{u}_i(t)]^2$. Here we neglect the statistical fluctuations of m_j in the velocity impulse and m_i in the energy density and assume them to be constant with the averaged value $\langle m_i\rangle$. The energy evolution of the system is then proportional to the quantity

$$P_{ij}(t)=[\dot{G}^{+}_{ij}(t)]^2 , \tag{2}$$

where G^+ is the retarded one-phonon Green's function for the displacement satisfying

$$m_i\ddot{G}^{+}_{ij}(t)+2dKG^{+}_{ij}(t)-K\sum_{l}{}'G^{+}_{lj}(t)=-2\pi\delta(t)\delta_{ij} , \tag{3}$$

with the same boundary condition described above. We now define the following Fourier transforms in time and space:

$$\begin{aligned} G^{+}_{ij}(E)&=\int_0^\infty dt\, e^{i(E+i\eta)t}G^{+}_{ij}(t) ,\\ G^{+}_{\mathbf{p},\mathbf{p}'}(E)&=\frac{1}{N}\sum_{i,j}e^{-i(\mathbf{p}\cdot\mathbf{R}_i-\mathbf{p}'\cdot\mathbf{R}_j)}G^{+}_{ij}(E) , \end{aligned} \tag{4}$$

where η is an infinitesimally positive number and $\mathbf{R}_i$ is the position vector of site i. The Fourier transform of Eq. (2) can be expressed as

$$\begin{aligned} P_{ij}(\omega)&=\int_0^\infty dt e^{i(\omega+i\eta)t}[\dot{G}^{+}_{ij}(t)]^2\\ &=\int_{-\infty}^{\infty}\frac{dE}{2\pi}\left[E+\frac{\omega}{2}\right]\left[E-\frac{\omega}{2}\right]\\ &\quad\times G^{+}_{ij}\left[E+\frac{\omega}{2}\right]G^{-}_{ij}\left[E-\frac{\omega}{2}\right] , \end{aligned} \tag{5}$$

where G^- is the corresponding advanced Green's function. Using the reciprocal relation $G^{-}_{ij}=G^{E}_{ji}$ and denoting the product

$$G^{+}_{ij}\left[E+\frac{\omega}{2}\right]G^{-}_{ji}\left[E-\frac{\omega}{2}\right]$$

by $P^{E}_{ij}(\omega)$, the configurationally averaged $P^{E}_{ij}(\omega)$ [denoted by $\bar{P}^{E}_{ij}(\omega)$] has the following Fourier transform in space

$$\begin{aligned} \bar{P}^{E}(\mathbf{q},\omega)&=\frac{1}{N}\sum_{i,j}e^{-i\mathbf{q}\cdot(\mathbf{R}_i-\mathbf{R}_j)}\bar{P}^{E}_{ij}(\omega)\\ &=\frac{1}{N}\sum_{\mathbf{p},\mathbf{p}'}\langle G^{+}_{\mathbf{p}_+,\mathbf{p}'_+}(E_+)G^{-}_{\mathbf{p}'_-,\mathbf{p}_-}(E_-)\rangle\\ &\equiv\frac{1}{N}\sum_{\mathbf{p},\mathbf{p}'}K^{E}_{\mathbf{p},\mathbf{p}'}(\mathbf{q},\omega) , \end{aligned} \tag{6}$$

where $E_\pm=E\pm\omega/2$ and $\mathbf{p}_\pm=\mathbf{p}\pm\mathbf{q}/2$. The nature of phonon states at any frequency E can be understood from the small-q and -w behavior of $\bar{P}^{E}(\mathbf{q},\omega)$. Extended states always lead to a diffusive pole in $\bar{P}^{E}(\mathbf{q},\omega)$. To find the explicit form of $\bar{P}^{E}(\mathbf{q},\omega)$ in the hydrodynamic limit, we first consider the problem within CPA.

In CPA, it is known that the averaged two-phonon Green's function $K^{E}_{\mathbf{p},\mathbf{p}'}(\mathbf{q},\omega)$ is given by[17–19]

$$K^{E}_{\mathbf{p},\mathbf{p}'}(\mathbf{q},\omega)=R^{+}_{\mathbf{p}_+}(E_+)R^{-}_{\mathbf{p}_-}(E_-)\left[\delta_{\mathbf{p},\mathbf{p}'}+\frac{L(E_+,E_-)/N}{1-\dfrac{L(E_+,E_-)}{N}\displaystyle\sum_{\mathbf{p}_1}R^{+}_{\mathbf{p}_{1+}}(E_+)R^{-}_{\mathbf{p}_{1-}}(E_-)}R^{+}_{\mathbf{p}'_+}(E_+)R^{-}_{\mathbf{p}'_-}(E_-)\right] . \tag{7}$$

In Eq. (7), $R^{\pm}_{\mathbf{p}}(E)$ is the averaged one-phonon Green's function which is determined by the following equations in CPA:[19,20]

$$\langle t^{\pm}_i\rangle=\left\langle\frac{[M^{\pm}(E)-m_i]E^2}{1-[M^{\pm}(E)-m_i]E^2R^{\pm}_{ii}(E)}\right\rangle=0 , \tag{8}$$

$$R^{\pm}_{ii}(E)=\frac{1}{N}\sum_{\mathbf{p}}R^{\pm}_{\mathbf{p}}(E) , \tag{9}$$

$$R^{\pm}_{\mathbf{p}}(E)=\frac{1}{M^{\pm}(E)E^2-\varepsilon(\mathbf{p})} . \tag{10}$$

$M^{\pm}(E)$ is the renormalized mass of the effective medium and $\varepsilon(\mathbf{p})=K\sum_\delta(1-e^{i\mathbf{p}\cdot\delta})$ with δ being the nearest-neighbor vectors. In the simple cubic lattice, with lattice constant a, $\varepsilon(\mathbf{p})$ equals

$$2K[3-\cos(p_xa)-\cos(p_ya)-\cos(p_za)] .$$

$L(E_+,E_-)$ in Eq. (7) is the effective two-phonon vertex in CPA and is given by

$$L(E_+,E_-)=\frac{\langle t^{+}_i(E_+)t^{-}_i(E_-)\rangle}{1+\langle t^{+}_i(E_+)t^{-}_i(E_-)\rangle R^{+}_{ii}(E_+)R^{-}_{ii}(E_-)} . \tag{11}$$

Using t^{+}_i of Eq. (8), it can be shown that $L(E_+,E_-)$ satisfies the following Ward identity in CPA

$$L(E_+,E_-)=\frac{(E_+E_-)^2[M^{+}(E_+)-M^{-}(E_-)]}{E^2_-R^{-}_{ii}(E_-)-E^2_+R^{+}_{ii}(E_+)} . \tag{12}$$

In the limit of small q and ω, we expand $R^{\pm}_{p_{1\pm}}(E_\pm)$ in Eq. (7) to second order in q, first order in ω, and $L(E_+,E_-)$ to the first order in ω. Using Eq. (12), after some manipulations, we obtain the following equation:

$$\frac{L(E_+,E_-)}{N}\sum_{\mathbf{p}_1} R^+_{\mathbf{p}_{1+}}(E_+)R^-_{\mathbf{p}_{1-}}(E_-)\simeq 1-\frac{2[R^+_{ii}(E)M^+(E)-R^-_{ii}(E)M^-(E)]}{E\Delta M(E)\Delta R_{ii}(E)]}\omega+\frac{\frac{1}{N}\sum_{\mathbf{p}} v^2(\mathbf{p})[\Delta R_{\mathbf{p}}(E)]^2}{2E^2 d\,\Delta M(E)\Delta R_{ii}(E)}q^2 ,$$

or

$$\frac{1}{1-\frac{L(E_+,E_-)}{N}\sum_{\mathbf{p}_1} R^+_{\mathbf{p}_{1+}}(E_+)R^-_{\mathbf{p}_{1-}}(E_-)}=\frac{1}{D_{\mathrm{CPA}}(E)q^2-i\omega}\left[\frac{-iE\Delta M(E)\Delta R_{ii}(E)}{2[R^+_{ii}(E)M^+(E)-R^-_{ii}(E)M^-(E)]}\right] \tag{13}$$

with

$$D_{\mathrm{CPA}}(E)=\frac{-1}{4\pi d\rho(E)}\frac{1}{N}\sum_{\mathbf{p}} v^2(\mathbf{p})[\Delta R_{\mathbf{p}}(E)]^2 , \tag{14}$$

$$\rho(E)=\frac{iE}{\pi}[M^+(E)R^+_{ii}(E)-M^-(E)R^-_{ii}(E)] , \tag{15}$$

$$\Delta M(E)=M^+(E)-M^-(E)=2i\ \mathrm{Im}M^+(E) , \tag{16}$$

$$\Delta R_{ii}(E)=R^+_{ii}(E)-R^-_{ii}(E)=2i\ \mathrm{Im}R^+_{ii}(E) , \tag{17}$$

$$\Delta R_{\mathbf{p}}(E)=R^+_{\mathbf{p}}(E)-R^-_{\mathbf{p}}(E)=2i\ \mathrm{Im}R^+_{\mathbf{p}}(E) , \tag{18}$$

and

$$\mathbf{v}(\mathbf{p})=\nabla_{\mathbf{p}}\varepsilon(\mathbf{p}) . \tag{19}$$

Notice that $\mathbf{v}(\mathbf{p})$ defined here is related but not equal to the phonon group velocity. $D_{\mathrm{CPA}}(E)$ is the diffusion constant in CPA. It can be shown that $\rho(E)$ of Eq. (15) is exactly the CPA phonon DOS which is defined as[20]

$$\rho(E)=\frac{-2E}{\pi}\mathrm{Im}\langle m_i G^+_{ii}(E)\rangle . \tag{20}$$

Substituting Eq. (7) into Eq. (6) and using Eq. (13), we obtain the expression for $\bar{P}^{\,E}(\mathbf{q},\omega)$ in CPA as

$$\bar{P}^{\,E}_{\mathrm{CPA}}(\mathbf{q},\omega)\cong\frac{1}{D_{\mathrm{CPA}}(E)q^2-i\omega}\left[\frac{-[\Delta R_{ii}(E)]^2}{2\pi\rho(E)}\right] . \tag{21}$$

Since $D_{\mathrm{CPA}}(E)$ is nonvanishing for all E in the band, we do not see any localization in CPA. In the next section, we will include the self-consistent treatment of coherent backscattering contributions to $\bar{P}^{\,E}(\mathbf{q},\omega)$ in order to obtain the localization effect.

III. SELF-CONSISTENT THEORY FOR LOCALIZATION

In this section, the self-consistent theory of VW is used in the context of CPA to study the properties of phonon localization. In general, the Bethe-Selpeter equation for $K^E_{\mathbf{p},\mathbf{p}'}(\mathbf{q},\omega)$ of Eq. (6) has the form

$$K^E_{\mathbf{p},\mathbf{p}'}(\mathbf{q},\omega)=R^+_{\mathbf{p}_+}(E_+)R^-_{\mathbf{p}_-}(E_-)\left[\delta_{\mathbf{p},\mathbf{p}'}+\frac{1}{N}\sum_{\mathbf{p}''} U^E_{\mathbf{p},\mathbf{p}''}(\mathbf{q},\omega)K^E_{\mathbf{p}'',\mathbf{p}'}(\mathbf{q},\omega)\right] , \tag{22}$$

with

$$U^E_{\mathbf{p},\mathbf{p}''}(\mathbf{q},\omega)=L(E_+,E_-)+\delta U^E_{\mathbf{p},\mathbf{p}''}(\mathbf{q},\omega) , \tag{23}$$

and

$$R^{\pm}_{\mathbf{p}}(E)=\frac{1}{M^{\pm}(E)E^2-\epsilon(\mathbf{p})-\Sigma^{\pm}(\mathbf{p},E)} . \tag{24}$$

Here, $\Sigma^{\pm}$ and δU are, respectively, the non-single-site diagram[19] contribution to the averaged one-phonon self-energy and the two-phonon vertex. Using the relation $R^+R^-=(R^+-R^-)/[(R^-)^{-1}-(R^+)^{-1}]$, Eq. (22) becomes

$$[E^2_-M^-(E_-)-E^2_+M^+(E_+)+\varepsilon(\mathbf{p}_+)-\varepsilon(\mathbf{p}_-)+\Sigma^+(\mathbf{p}_+,E_+)-\Sigma^-(\mathbf{p}_-,E_-)]K^E_{\mathbf{p},\mathbf{p}'}(\mathbf{q},\omega)$$
$$=\Delta R^E_{\mathbf{p}}(\mathbf{q},\omega)\left[\delta_{\mathbf{p},\mathbf{p}'}+\frac{1}{N}\sum_{\mathbf{p}''}[L(E_+,E_-)+\delta U^E_{\mathbf{p},\mathbf{p}''}(\mathbf{q},\omega)]K^E_{\mathbf{p}'',\mathbf{p}'}(\mathbf{q},\omega)\right] , \tag{25}$$

where

$$\Delta R^E_{\mathbf{p}}(\mathbf{q},\omega)=R^+_{\mathbf{p}_+}(E_+)-R^-_{\mathbf{p}_-}(E_-) .$$

Summing Eq. (25) on $\mathbf{p}$ and $\mathbf{p}'$ and using Eq. (6), we find, to the lowest order in q, the following equation

$$[E^2_-M^-(E_-)-E^2_+M^+(E_+)]\bar{P}^{\,E}(\mathbf{q},\omega)+q\bar{P}^{\,E}_j(\mathbf{q},\omega)=\Delta R^E_{ii}(0,\omega)[1+L(E_+,E_-)\bar{P}^{\,E}(\mathbf{q},\omega)] , \tag{26}$$

where we have defined the current relaxation function as

$$\bar{P}_j^E(\mathbf{q},\omega)=\frac{1}{N}\sum_{\mathbf{p},\mathbf{p}'}[\mathbf{v}(\mathbf{p})\cdot\hat{\mathbf{q}}]K^E_{\mathbf{p},\mathbf{p}'}(\mathbf{q},\omega) \tag{27}$$

and

$$\Delta R_{ii}^E(\mathbf{q},\omega)=\frac{1}{N}\sum_{\mathbf{p}}\Delta R_{\mathbf{p}}^E(\mathbf{q},\omega)\ . \tag{28}$$

In the derivation of Eq. (26), we have made use of the following Ward identity for the non-single-site diagrams:

$$\Sigma^+(\mathbf{p}_+,E_+)-\Sigma^-(\mathbf{p}_-,E_-)=\sum_{\mathbf{p}'}\delta U^E_{\mathbf{p},\mathbf{p}'}(\mathbf{q},\omega)\Delta R^E_{\mathbf{p}'}(\mathbf{q},\omega)\ . \tag{29}$$

The above relation is required by the conservation law. In order to derive an equation for $\bar{P}_j^E(\mathbf{q},\omega)$ (current relaxation equation), the function $\sum_{\mathbf{p}'}K^E_{\mathbf{p},\mathbf{p}'}(\mathbf{q},\omega)$ is expanded in angular variable. In the strong-coupling limit, we use the following expansion[5,21]

$$\sum_{\mathbf{p}'}K^E_{\mathbf{p},\mathbf{p}'}(\mathbf{q},\omega)=\frac{\Delta R^E_{\mathbf{p}}(0,\omega)}{\Delta R^E_{ii}(0,\omega)}\frac{1}{N}\sum_{\mathbf{p}'',\mathbf{p}'}K^E_{\mathbf{p}'',\mathbf{p}'}(\mathbf{q},\omega)+\frac{[\Delta R^E_{\mathbf{p}}(0,\omega)]^2[\mathbf{v}(\mathbf{p})\cdot\hat{\mathbf{q}}]}{\frac{1}{N}\sum_{\mathbf{p}'}[\Delta R^E_{\mathbf{p}'}(0,\omega)\mathbf{v}(\mathbf{p}')\cdot\hat{\mathbf{q}}]^2}\frac{1}{N}\sum_{\mathbf{p}'',\mathbf{p}'}(\mathbf{v}(\mathbf{p}'')\cdot\hat{\mathbf{q}})K^E_{\mathbf{p}'',\mathbf{p}'}(\mathbf{q},\omega)\ . \tag{30}$$

Multiplying Eq. (25) by $\mathbf{v}(\mathbf{p})\cdot\hat{\mathbf{q}}$ and summing $\mathbf{p}$ and $\mathbf{p}'$, we find

$$[E_-^2M^-(E_-)-E_+^2M^+(E_+)+Q^E(\mathbf{q},\omega)]\bar{P}_j^E(\mathbf{q},\omega)-\mathcal{L}^E(\mathbf{q},\omega)\bar{P}^E(\mathbf{q},\omega)=\frac{1}{N}\sum_{\mathbf{p}}\Delta R^E_{\mathbf{p}}(\mathbf{q},\omega)[\mathbf{v}(\mathbf{p})\cdot\hat{\mathbf{q}}]\ , \tag{31}$$

with

$$Q^E(\mathbf{q},\omega)=\frac{\frac{-1}{N^2}\sum_{\mathbf{p},\mathbf{p}'}[\mathbf{v}(\mathbf{p})\cdot\hat{\mathbf{q}}]\Delta R^E_{\mathbf{p}}(\mathbf{q},\omega)\delta U^E_{\mathbf{p}\mathbf{p}'}(\mathbf{q},\omega)[\Delta R^E_{\mathbf{p}'}(0,\omega)]^2[\mathbf{v}(\mathbf{p}')\cdot\hat{\mathbf{q}}]}{\frac{1}{dN}\sum_{\mathbf{p}'}[\Delta R^E_{\mathbf{p}'}(0,\omega)]^2v^2(\mathbf{p}')}\ , \tag{32}$$

and

$$\mathcal{L}^E(\mathbf{q},\omega)=\frac{-q}{\Delta R^E_{ii}(0,\omega)}\frac{1}{N}\sum_{\mathbf{p}}\Delta R^E_{\mathbf{p}}(0,\omega)[\mathbf{v}(\mathbf{p})\cdot\hat{\mathbf{q}}]^2+\frac{L(E_+,E_-)}{N}\sum_{p}\Delta R^E_{\mathbf{p}}(\mathbf{q},\omega)[\mathbf{v}(\mathbf{p})\cdot\hat{\mathbf{q}}]\ . \tag{33}$$

In the derivation of Eq. (31), Eq. (30) has been used and we have ignored $\Sigma^{\pm}$ terms in Eq. (25) and δU term in $\mathcal{L}^E(\mathbf{q},\omega)$ of Eq. (33) for practical purpose. Thus, we will again use Eq. (10) as the CPA of $R^{\pm}_{\mathbf{p}}(E)$. Solving Eqs. (26) and (31) for $\bar{P}^E(\mathbf{q},\omega)$ yields, to the lowest order in q,

$$\bar{P}^E(\mathbf{q},\omega)\cong\frac{\Delta R^E_{ii}(0,\omega)}{E_-^2M^-(E_-)-E_+^2M^+(E_+)-L(E_+,E_-)\Delta R^E_{ii}(0,\omega)+\frac{q\mathcal{L}^E(q,\omega)}{E_-^2M^-(E_-)-E_+^2M^+(E_+)+Q^E(0,\omega)}}\ . \tag{34}$$

By expanding $\Delta R^E_{\mathbf{p}}(\mathbf{q},\omega)$ to the first order in q, it can be shown that $\mathcal{L}^E(\mathbf{q},\omega)$ of Eq. (33), to the lowest order in q and ω, is given by

$$\mathcal{L}^E(\mathbf{q},\omega)\cong 2\pi qD_{\mathrm{CPA}}(E)\Delta M(E)E^2\rho(E)/\Delta R_{ii}(E) \tag{35}$$

Thus, to the lowest order in w, using Eq. (35) and Eq. (13) with $q=0$, Eq. (34) reduces to

$$\bar{P}^E(\mathbf{q},\omega)\cong\frac{1}{D(E,\omega)q^2-i\omega}\left[\frac{-[\Delta R_{ii}(E)]^2}{2\pi\rho(E)}\right] \tag{36}$$

with

$$D(E,\omega)\cong\frac{D_{\mathrm{CPA}}(E)}{1-\frac{Q^E(0,\omega)}{E^2\Delta M(E)}}\ , \tag{37}$$

where the DOS $\rho(E)$ is given by Eq. (15). Equation (36) has exactly the same form as Eq. (21) except that the CPA diffusion constant is now replaced by a renormalized one which is to be determined self-consistently. Following VW, we include only the maximally crossed diagrams in the term δU of $Q^E(\mathbf{q},\omega)$ of Eq. (32). Using time-reversal symmetry, these diagrams can be summed by using Eq. (13), yielding

$$\delta U^{E}_{\mathbf{p},\mathbf{p}'}(0,\omega)\cong\frac{1}{D_{\mathrm{CPA}}(E)\,|\,\mathbf{p}+\mathbf{p}'\,|^{2}-i\omega}\left[\frac{-E^{4}[\Delta M(E)]^{2}}{2\pi\rho(E)}\right]. \tag{38}$$

Substituting Eq. (38) into Eq. (32), the leading term in $Q^{E}(0,\omega)$ gives

$$Q^{E}(0,\omega)\cong\frac{-E^{4}[\Delta M(E)]^{2}\sum_{\mathbf{p}}v^{2}(\mathbf{p})[\Delta R_{\mathbf{p}}(E)]^{2}}{2\pi\rho(E)\sum_{\mathbf{p}}v^{2}(\mathbf{p})[\Delta R_{\mathbf{p}}(E)]^{2}}\frac{1}{N}\sum_{\mathbf{q}}\frac{1}{D_{\mathrm{CPA}}(E)q^{2}-i\omega}. \tag{39}$$

Replacing $D_{\mathrm{CPA}}(E)$ in Eq. (39) by $D(E,\omega)$ and substituting Eq. (39) into Eq. (37), we obtain the self-consistent equation for the diffusion constant $D(E,\omega)$ as

$$D(E,\omega)=D_{\mathrm{CPA}}(E)-\frac{S(E)}{\pi\rho(E)D_{\mathrm{CPA}}(E)}\frac{1}{N}\sum_{\mathbf{q}}\frac{1}{q^{2}-\dfrac{i\omega}{D(E,\omega)}}, \tag{40}$$

with

$$S(E)=\frac{-E^{2}\Delta M(E)}{8d\pi\rho(E)}\frac{1}{N}\sum_{\mathbf{p}}v^{2}(\mathbf{p})[\Delta R_{\mathbf{p}}(E)]^{3}. \tag{41}$$

Equations (40) and (41) are identical in forms to the self-consistent equation for the conductivity in the tight-binding electron model.[5] Equation (40) gives the known result that all states are localized in systems with dimension $d\leq 2$ except the Goldstone mode at $E=0$.

IV. MODEL ASSUMPTIONS AND ANALYTIC RESULTS

Here we consider the three-dimensional case. Since we are only interested in the dc behavior, we take $\omega\rightarrow 0^{+}$ limit in the discussions below. In the extended states region, Eq. (40) gives the following diffusion constant

$$D(E)\equiv D(E,0^{+})=D_{\mathrm{CPA}}(E)-\frac{S(E)q_{c}}{2\pi^{3}\rho(E)D_{\mathrm{CPA}}(E)}, \tag{42}$$

where q_c is the upper momentum cutoff. Equation (42) can be written as

$$D(E)=D_{\mathrm{CPA}}(E)[1-\chi(E)], \tag{43}$$

with

$$\chi(E)=\frac{S(E)q_{c}}{2\pi^{3}\rho(E)[D_{\mathrm{CPA}}(E)]^{2}}. \tag{44}$$

The mobility edge is determined by the condition $D(E^{*})=0$ [or $\chi(E^{*})=1$]. In the localized region, it is known that $D(E,\omega)$ is related to the localization length ξ_{loc} by[16]

$$D(E,\omega)\cong-i\omega\xi^{2}_{\mathrm{loc}}(E)+O(\omega^{2}). \tag{45}$$

Substituting Eq. (45) into Eq. (40), we have the equation for ξ_{loc} as

$$\xi_{\mathrm{loc}}(E)q_{c}\{\tan^{-1}[\xi_{\mathrm{loc}}(E)q_{c}]\}^{-1}=[1-\chi(E)]^{-1}. \tag{46}$$

In the extended region, the correlation length ξ_{cor} can be defined as[8]

$$\xi_{\mathrm{cor}}(E)=\frac{l_{F}(E)D_{\mathrm{CPA}}(E)}{D(E)}=\frac{l_{F}(E)}{1-\chi(E)}, \tag{47}$$

where l_F is the mean free path of the phonon. From Eqs. (46) and (47), it is easily seen that both ξ_{loc} and ξ_{cor} diverge at the mobility edge with an exponent one, i.e., $\xi_{\mathrm{loc}}(E)$ [or $\xi_{\mathrm{cor}}(E)$] $\propto|E-E^{*}|^{-1}$. The mean free path l_F can be defined as

$$l_{F}(E)=\frac{3D_{\mathrm{CPA}}(E)}{v_{0}(E)}. \tag{48}$$

Here, $v_0(E)$ is the mean group velocity of the phonons which can be defined as follows. Since $\mathrm{Im}R^{+}_{\mathbf{p}}(E)$ has a peak around $E=E_{\mathbf{p}}$ with $E^{2}_{\mathbf{p}}\mathrm{Re}[M^{+}(E_{\mathbf{p}})]=\varepsilon(\mathbf{p})$, the group velocity is given by

$$\mathbf{v}_{g}(\mathbf{p})=\nabla_{\mathbf{p}}E_{\mathbf{p}}=\frac{\nabla_{\mathbf{p}}\varepsilon(\mathbf{p})}{2E_{\mathbf{p}}\mathrm{Re}M^{+}(E_{\mathbf{p}})+E^{2}_{\mathbf{p}}\dfrac{\partial}{\partial E_{\mathbf{p}}}[\mathrm{Re}M^{+}(E_{\mathbf{p}})]}. \tag{49}$$

After averaging over $\mathbf{p}$ and weighted by the spectral density, $\mathbf{v}_0(E)$ can be defined as

$$v^{2}_{0}(E)=\frac{-2E}{\pi\rho(E)\left[2E\,\mathrm{Re}M^{+}(E)+E^{2}\dfrac{\partial}{\partial E}[\mathrm{Re}\,M^{+}(E)]\right]^{2}}\times\frac{1}{N}\sum_{\mathbf{p}}v^{2}(\mathbf{p})\mathrm{Im}[M^{+}(E)R^{+}_{\mathbf{p}}(E)]. \tag{50}$$

In our numerical calculations, we use the semi-elliptical band approximation. Defining $W=6K$, $\bar{\varepsilon}(\mathbf{p})=W-\varepsilon(\mathbf{p})$, and using the following ansätze,[18,22]

$$\begin{aligned}\frac{1}{N}\sum_{\mathbf{p}}\delta(y-\bar{\varepsilon}(\mathbf{p}))&=\frac{2}{\pi W}\left[1-\left[\frac{y}{W}\right]\right]^{1/2}\Theta(W-|\,y\,|),\\ \frac{1}{N}\sum_{\mathbf{p}}\delta(y-\bar{\varepsilon}(\mathbf{p}))[\mathbf{v}(p)]^{2}&=\frac{2W}{3\pi}\left[1-\left[\frac{y}{W}\right]^{2}\right]^{3/2}\times\Theta(W-|\,y\,|),\end{aligned} \tag{51}$$

the $\mathbf{p}$ summation in Eqs. (9), (14), (50), and (41) can be performed analytically yielding

$$R_{ii}^{\pm}(E)=\frac{2}{W^2}(M^{\pm}(E)E^2-W-\{M^{\pm}(E)E^2[M^{\pm}(E)E^2-2W]\}^{1/2}) , \tag{52}$$

$$D_{\mathrm{CPA}}(E)=\frac{1}{9\pi\rho(E)}\left[1+\frac{\pi\rho(E)}{2EM_I(E)}\left[W-\frac{E^2M_R(E)}{2}\right]-E^2\mathrm{Re}[M^+(E)R_{ii}^+(E)]+\tfrac{3}{2}W\,\mathrm{Re}R_{ii}^+(E)\right] , \tag{53}$$

$$\begin{aligned}v_0^2(E)=&\{2M_I(E)[W-2M_R(E)E^2]+2\pi WE\rho(E)M_R(E)+\pi E^3\rho(E)[M_I^2(E)-M_R^2(E)]\\&+4M_I(E)E^2\mathrm{Re}[M^+(E)R_{ii}^+(E)][M_R(E)E^2-W]\}\Big/3\pi E\rho(E)\left[2M_R(E)+E\frac{\partial M_R(E)}{\partial E}\right]^2 ,\end{aligned} \tag{54}$$

and

$$\begin{aligned}S(E)=\frac{1}{6\pi\rho(E)}&\left[9\pi\rho(E)D_{\mathrm{CPA}}(E)+\frac{\pi}{4}E\rho(E)[M_I(E)E^2A_R(E)-WA_I(E)]\right.\\&+M_I(E)E^2A_I(E)+\frac{E^2}{2}[WM_I(E)A_R(E)-WM_R(E)A_I(E)-M_I(E)]\\&\left.\times\mathrm{Im}R_{ii}^+(E)-\frac{E^4}{2}A_I(E)M_I(E)\mathrm{Re}[M^+(E)R_{ii}^+(E)]\right] ,\end{aligned} \tag{55}$$

with

$$A_R(E)=\mathrm{Re}\left[\frac{M^+(E)E^2-W}{M^+(E)E^2[M^+(E)E^2-2W]}\right] \tag{56}$$

and

$$A_I(E)=\mathrm{Im}\left[\frac{M^+(E)E^2-W}{M^+(E)E^2[M^+(E)E^2-2W]}\right] , \tag{57}$$

where M_R and M_I are, respectively, the real and imaginary parts of M^+. Now, the effective-medium mass $M^+(E)$ is determined by Eqs. (8) and (52). Using the Eqs. (52)–(57) in Eqs. (15), (42), (46), (47), and (48), all the physical quantities we are interested in here can be calculated directly. Although the above results are general for any n-component mixed crystal, our numerical calculations will be limited to two components only.

For a two-component system, $M^+(E)$ [or $R_{ii}^+(E)$] which is determined by Eqs. (8) and (52) satisfies a cubic equation and can be solved analytically.[23] There is a reciprocal relation in the phase space of mass ratio and concentration. Let the mass of the two components be m and αm with the corresponding concentrations $1-c$ and c. If we write Eq. (1) in the frequency space, the same equation can describe a reciprocal system having the masses m/α and m with the corresponding concentrations $1-c$ and c if the frequency E is scaled by a factor $\sqrt{\alpha}$; i.e., $E'=\sqrt{\alpha}E$. So, we will only consider the region $\alpha>1$. Before giving the numerical results, we consider two limiting cases; the small-frequency limit and the infinite-α limit.

In the low-frequency limit, there are always extended states for any finite value of α and the whole range of c. The case when α is infinite is an exception. The reasons will be given later. By solving CPA Eqs. (8) and (52) in the $E\to 0$ limit and using Eqs. (15) and (53)–(57), the following asymptotic behaviors are known for small E:

$$\rho(E)\cong\frac{4\overline{m}}{\pi W^2}\sqrt{2W\overline{m}}\,E^2 , \tag{58}$$

$$D_{\mathrm{CPA}}(E)\cong\frac{W^3}{36\sqrt{2W\overline{m}}\,m^2(1-\alpha)^2c(1-c)}E^{-4} , \tag{59}$$

$$v_0^2(E)\cong\frac{Wm^2[(1-c)(2-c+2\alpha c)+\alpha^2c(1+c)]}{12\overline{m}^3} , \tag{60}$$

and

$$S(E)\cong\tfrac{3}{2}D_{\mathrm{CPA}}(E) , \tag{61}$$

with

$$\overline{m}\equiv\langle m_i\rangle=m(1-c+\alpha c) . \tag{62}$$

Using Eqs. (58)–(61), we find, for small E, $x(E)\propto E^2$, $l_F(E)\propto E^{-4}$, and $\xi_{\mathrm{cor}}(E)\propto E^{-4}$ from Eqs. (44), (48), and (47). Thus, there are always extended states in small frequency region.

In the limit when α becomes infinite, an explicit expression for $M^+(E)$ can also be obtained. In this case, Eq. (8) becomes

$$[M^+(E)-m]E^2R_{ii}^+(E)=c . \tag{63}$$

By solving Eqs. (52) and (63) for $M^+(E)$, we find

$$M^+(E)E^2=mE^2+\frac{cW}{2(1-c)}\left[\frac{mE^2}{W}-1+\sqrt{c-b(E)}\right] , \tag{64}$$

with

$$b(E)=1-\left[\frac{mE^2}{W}-1\right]^2 . \tag{65}$$

From Eqs. (64) and (65), we find that the DOS is nonvanishing only in the region $1-\sqrt{1-c}<mE^2/W<1+\sqrt{1-c}$. Having Eq. (64) for $M^+(E)$, the expressions for other interested quantities can also be obtained

by straightforward manipulations. We find

$$R_{ii}^{+}(E)=\frac{2}{W}\left[\frac{mE^2}{W}-1-\sqrt{c-b(E)}\right], \tag{66}$$

$$\rho(E)=\frac{4mE}{\pi W}\sqrt{b(E)-c}\,\Theta(b(E)-c), \tag{67}$$

$$D_{\mathrm{CPA}}(E)=\frac{1}{9\pi\rho(E)}\left[1+\frac{2}{c}\right][b(E)-c]\Theta(b(E)-c), \tag{68}$$

$$v_0^2(E)=\frac{W}{3m}\left[\frac{1-c}{2-c}\right]^2\left[\frac{W}{mE^2}\right]^2 \times\left[\frac{c}{4}+\left[b(E)-\frac{c}{2}\right]\frac{mE^2}{W}\right]\Theta(b(E)-c), \tag{69}$$

and

$$S(E)=\frac{1}{6\pi\rho(E)} \times\left[1+\frac{2}{c}+\frac{c}{2(1-c)}\left[1+\frac{4b(E)-4-2c+c^2}{4[b(E)-c]+c^2}\right]\right] \times[b(E)-c]\Theta(b(E)-c). \tag{70}$$

V. NUMERICAL RESULTS AND DISCUSSIONS

In our numerical calculations we have set the mass $m=1$, the force constant $K=1$ and the lattice constant $a=1$. The choice of q_c in Eq. (42) can be either $\beta\pi$ or $\beta\pi/l_F$ with β being of the order of 1.[5,7] Here, we take $\beta=1$. In the following, we will use superscripts (or subscripts) I and II respectively for the quantities calculated using $q_c^{\mathrm{I}}=\pi$ and $q_c^{\mathrm{II}}=\pi/l_F$. As mentioned in Sec. IV, it is sufficient to consider only the region $\alpha>1$. In this region, our results show that there exists a critical value of α^*. For $1<\alpha<\alpha^*$ ($\alpha_{\mathrm{I}}^*=1.75$ and $\alpha_{\mathrm{II}}^*=1.55$), there is only one mobility edge in the whole band for the whole range of concentration. In Fig. 1, we plot the $\rho(E)$, $v_0(E)$, and $D_{\mathrm{CPA}}(E)$ for a typical case $\alpha=1.4$ and $c=0.5$. In the small frequency region, these curves follow Eqs. (58)–(60). The curves $D_{\mathrm{I}}(E)$ and $D_{\mathrm{II}}(E)$ are indistinguishable from the curve $D_{\mathrm{CPA}}(E)$ on the scale shown in Fig. 1. We also plot the reduction factor $1-x_{\mathrm{I}}(E)$ [and $1-x_{\mathrm{II}}(E)$] in Fig. 1. In this case, the localization effect is significant only in the region of the band edge. In this range of α, the mobility edge moves from the band edge of the mass 1 system toward lower frequency as c is increased from zero. As c is closed to 1, the mobility edge lies near the band edge of the pure mass α system.

For $\alpha>\alpha^*$, multimobility edges appear in certain range of concentration. Results from a typical case $\alpha=3$ are shown in Figs. 2, 3, and 4 for $c=0.1$, 0.5, and 0.75. In these figures, the curves for $\rho(E)$, $D_{\mathrm{I}}(E)$, and $D_{\mathrm{II}}(E)$ are shown. In this region, for any value of α there exists a critical concentration $c_1^*(\alpha)$. The value of c_1^* ($\alpha=3$) is 0.220 when q_c^{I} is used and 0.124 when q_c^{II} is used. When

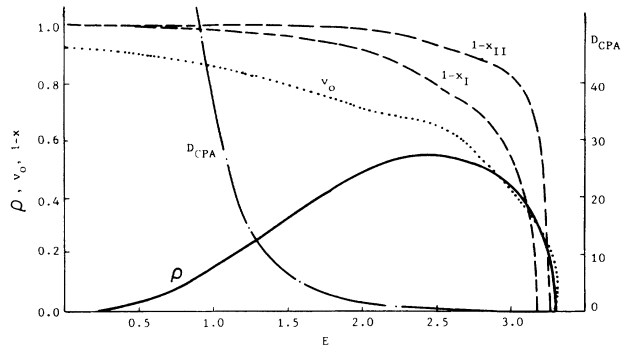

FIG. 1. The density of states per site (in units of $\sqrt{m/K}$; see text) ρ (——), CPA diffusion constant (in units of $\sqrt{K/m}\,a^2$) D_{CPA} (—·—), mean velocity (in units of $\sqrt{K/m}\,a$) v_0 (· · · ·), reduction factor $1-x_{\mathrm{I}}$ (— — —) (for $q_c^{\mathrm{I}}=\pi/a$), and $1-x_{\mathrm{II}}$ (— — —) (for $q_c^{\mathrm{II}}=\pi/l_F$) plotted against the frequency (in units of $\sqrt{K/m}$) E for the case $\alpha=1.4$ and $c=0.5$.

$c<c_1^*(\alpha)$, there is only one mobility edge in the system which lies near the band edge (Fig. 2). The band is not split. As c is increased to $c_1^*(\alpha)$, localized states appear at a single isolated frequency $E_1^{**}(\alpha)$ in the originally extended region. The value of $E_1^{**}(\alpha=3)$ is 1.48 when q_c^{I} is used and 1.33 when q_c^{II} is used. At this isolated frequency, the correlation lengths diverge from both sides with an exponent $\nu=2$ which is different from the exponent at usual mobility edge ($\nu=1$). The reason for this new exponent is because at this critical $c_1^*(\alpha)$ two roots of $x(E)=1$ coincide at E_1^{**} and this makes $x'(E_1^{**})=0$. The α dependence of the isolated frequency $E_1^{**}(\alpha)$ can be understood as follows. The function $c_1^*(\alpha)$ is a monotonically decreasing function of α as will be shown later in Fig. 7. When α is large enough (>2.7) such that $c_1^*(\alpha)$ is smaller than 0.25, the localization is due to the scattering of the phonon in the light mass host by the heavy mass impurities and the localization frequency $E_1^{**}(\alpha)$ is strongly related to the resonance scattering of the impurities. Since the concentration is small, the typical resonance frequency is the nature frequency of a single impurity with mass α which has the value

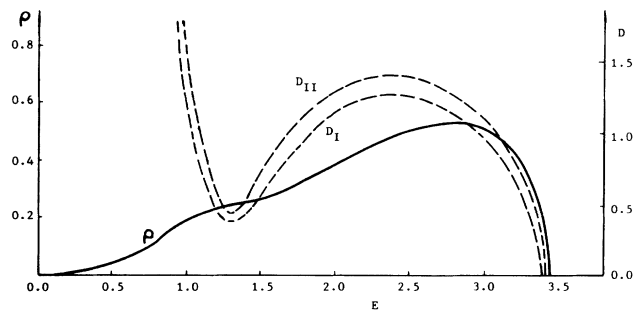

FIG. 2. The density of states per site (in units of $\sqrt{m/K}$) ρ (——), diffusion constant (in units of $\sqrt{K/m}\,a^2$) D_{I} (— — —) (for $q_c^{\mathrm{I}}=\pi/a$), and D_{II} (— — —) (for $q_c^{\mathrm{II}}=\pi/l_F$) plotted against the frequency (in units of $\sqrt{K/m}$) E for the case $\alpha=3$ and $c=0.1$.

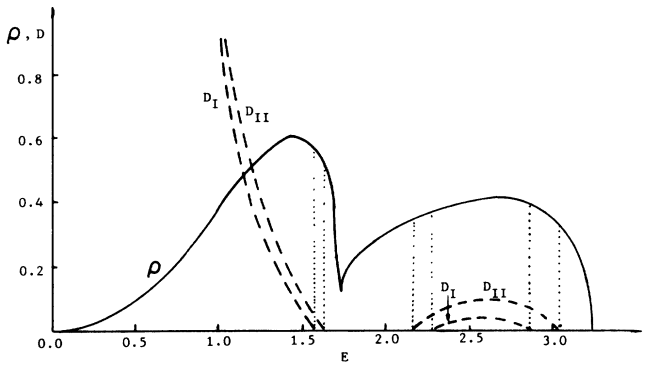

FIG. 3. The density of states per site (in units of $\sqrt{m/K}$) ρ (——), diffusion constant (in units of $\sqrt{K/m}\,a^2$) $D_{\rm I}$ (— — —) (for $q_c^{\rm I}=\pi/a$), and $D_{\rm II}$ (— — —) (for $q_c^{\rm II}=\pi/l_F$) plotted against the frequency (in units of $\sqrt{K/m}$) E for the case $\alpha=3$ and $c=0.5$. The position of the dashed lines on the frequency axis are the mobility edges calculated by using both $q_c^{\rm I}$ and $q_c^{\rm II}$.

$E_r(\alpha)=\sqrt{2d/\alpha}$. We have compared several values of $E_r(\alpha)$ with the corresponding values of $E_1^{**}(\alpha)$ and the agreement is good. For instance when $\alpha=3$, the value of $E_r(3)$ is 1.41 which lies just between the values 1.48 and 1.33 obtained for $E_1^{**}(3)$ by using $q_c^{\rm I}$ and $q_c^{\rm II}$, respectively. When α is small ($\alpha^*<\alpha<2.7$) and $c_1^*(\alpha)$ is larger than 0.25, the value of $E_r(\alpha)$ becomes smaller than the value of $E_1^{**}(\alpha)$ and the deviation is larger as α is smaller. In this region the effective medium should be used as the host instead of the light mass atoms, and the value of α in $\sqrt{2d/\alpha}$ should be replaced by a smaller effective value due to a smaller contrast. As c is increased beyond $c_1^*(\alpha)$, a finite localized region together with a new pair of mobility edge appears near E_1^{**} (Fig. 3). With c further increased, the upper bound of this newly localized region moves toward higher frequency, and the mobility

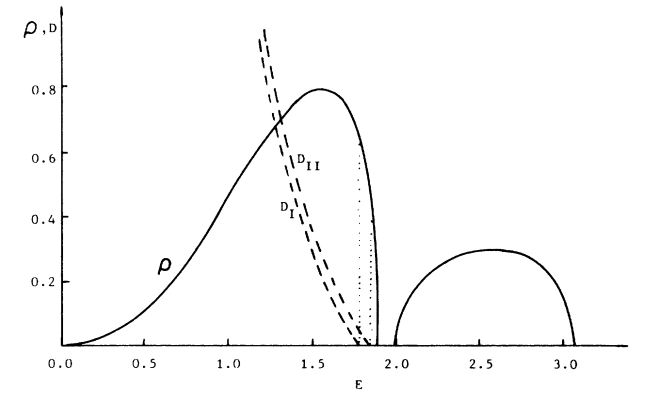

FIG. 4. The density of states per site (in units of $\sqrt{m/K}$) ρ (——), diffusion constant (in units of $\sqrt{K/m}\,a^2$) $D_{\rm I}$ (— — —) (for $q_c^{\rm I}=\pi/a$), and $D_{\rm II}$ (— — —) (for $q_c^{\rm II}=\pi/l_F$) plotted against the frequency (in units of $\sqrt{K/m}$) E for the case $\alpha=3$ and $c=0.75$. The position of the dashed lines on the frequency axis are the mobility edges calculated by using both $q_c^{\rm I}$ and $q_c^{\rm II}$.

edge of the originally localized region on the higher-frequency side moves toward lower frequency. These two mobility edges merge when c reaches to another critical $c_2^*(\alpha)$. In this case, the entire extended region on the higher-frequency side disappears. For the same reason discussed previously, the frequency $E_2^{**}(\alpha)$ where two mobility edges coincide is also a special frequency at which the localization lengths diverge from both sides with an exponent two ($\nu=2$). The value of $c_2^*(\alpha=3)$ is 0.547 when $q_c^{\rm I}$ is used and 0.604 when $q_c^{\rm II}$ is used. The corresponding value for E_2^{**} ($\alpha=3$) is 2.60 for $q_c^{\rm I}$ and 2.64 for $q_c^{\rm II}$. As c is increased beyond $c_2^*(\alpha)$, only one extended region exists on the lower-frequency side. The mobility edge lies near the band edge of the pure mass α system and the band is generally split (Fig. 4). In this region of c [$c_2^*(\alpha)<c<1$], the extended states are mainly supported by the heavy mass α and the light mass ($m=1$) contribute mainly to the localized modes on the higher-frequency subband. This is also the regime where the classical percolation theory applies.[13] According to the percolation concept, when $c>1-p_c\cong 0.69$ ($p_c\cong 0.31$ for the site percolation on simple cubic lattice), the light mass do not percolate and forming isolated clusters embedded in the infinite cluster of the heavy mass. The extended states on the lower-frequency side are supported by the infinite cluster together with the resonance modes of the finite clusters. However, on the higher-frequency side, there are only localized modes which is supported solely by the isolated clusters of the light mass. Thus, the mobility edge in this region [$c>c_2^*(\alpha)$] will move toward lower frequency as α is increased. Finally all states become localized when α is infinite. In the above discussions, the change of ν at E_1^{**} (or E_2^{**}) is related to our definition of $\xi_{\rm cor}$ (or $\xi_{\rm loc}$) $\sim |E-E^*|^{-\nu}$. It is quite possible that the change of ν at E_1^{**} (or E_2^{**}) is not genuine and is similar to the Anderson transition which occurred in the tight-binding electron case.[24,25] If so, new scaling fields are required to define the divergent of $\xi_{\rm cor}$ (or $\xi_{\rm loc}$) at E_1^{**} (or E_2^{**}) and the corresponding value of ν will be unchanged. While keeping in mind the above possibility, the exponent ν in this work is always defined as $\xi_{\rm cor}$ (or $\xi_{\rm loc}$) $\sim |E-E^*|^{-\nu}$ for convenience.

When α is infinite, for any c only zero-frequency mode can be supported by the infinite mass and all the states in the band are due to the light mass. The band is bounded by $1-\sqrt{1-c}<E^2/6<1+\sqrt{1-c}$ under CPA. When c is small, two mobility edges appear near the lower and upper band edges (Fig. 5). With increasing c these two mobility edges move toward each other and they merge when c reaches $c_2^*(\alpha=\infty)$ which has the value of 0.522 when $q_c^{\rm I}$ is used and 0.620 when $q_c^{\rm II}$ is used. All states are localized when $c>c_2^*(\infty)$. The infinite α limit considered here does not correspond to the usual percolation limit. In the later case, these is no interaction between the two nearby components and the problem is pure off-diagonal randomness in nature. However, in our purely diagonal randomness model a constant force is exerted on the light mass by the nearby infinite mass. Thus, we do not obtain here a region of extended states in the small frequency region as we always do in the percolation sys-

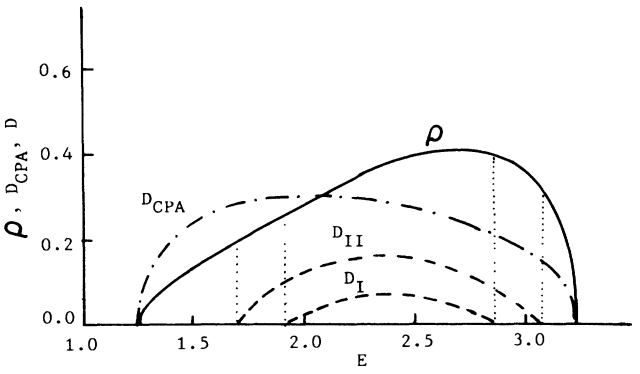

FIG. 5. The density of states per site (in units of $\sqrt{m/K}$) ρ (——), CPA diffusion constant (in units of $\sqrt{K/m}\,a^2$) $D_{\rm CPA}$ (—·—), diffusion constant (in units of $\sqrt{K/m}\,a^2$) $D_{\rm I}$ (— — —) (for $q_c^{\rm I}=\pi/a$), and $D_{\rm II}$ (— — —) (for $q_c^{\rm II}=\pi/l_F$), plotted against the frequency (in units of $\sqrt{K/m}$) E for the case $\alpha=\infty$ and $c=0.45$. The position of the dotted lines on the frequency axis are the mobility edges calculated by using both $q_c^{\rm I}$ and $q_c^{\rm II}$.

tem whenever the light mass percolates.[26] In Fig. 5 we plot $\rho(E)$, $D_{\rm I}(E)$, and $D_{\rm II}(E)$ for the case $c=0.45$. From Figs. 1–5, we find that the choice of two different values of q_c makes only quantitative changes to all the physical properties considered here. In Fig. 6, we plot the correlation and localization lengths for a typical case $\alpha=3$ and $c=0.5$ using $q_c^{\rm I}=\pi$.

The above discussions can be summarized using Fig. 7. In Fig. 7, two isolated regions are identified in (α,c) space. The region Q is obtained from the region P by using reciprocal relation, i.e., $\alpha\rightarrow 1/\alpha$ and $c\rightarrow 1-c$. Outside these regions there is only one mobility edge in the system and this mobility edge moves continuously in the frequency space as c and α vary. Inside these regions, there are three mobility edges in the system. On the boundaries of these regions, as we cross the critical line

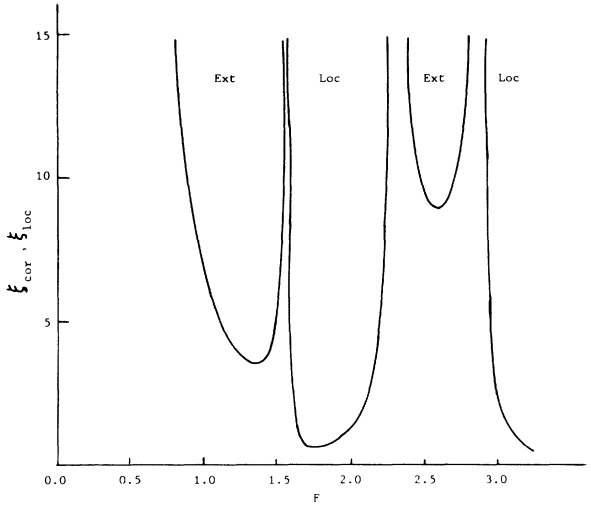

FIG. 6. The correlation and localization length (in units of a) obtained by using $q_c^{\rm I}$ plotted against the frequency (in units of $\sqrt{K/m}$) for the case $\alpha=3$ and $c=0.5$.

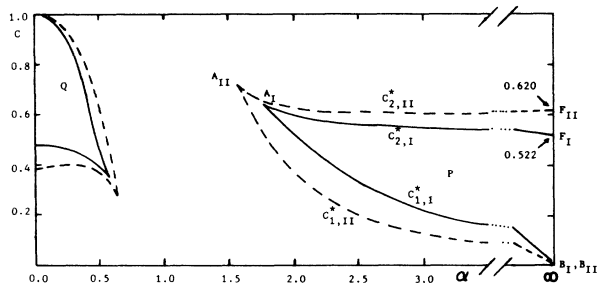

FIG. 7. Two isolated regions P and Q shown in the (α,c) space. Inside these regions, there are three mobility edges in the system. Outside these regions, there is only one mobility edge in the system. The correlation and localization lengths diverge, respectively, on the critical lines AB and AF. The point A is a critical point of higher order. Subscripts I and II are used for the boundaries calculated using $q_c^{\rm I}=\pi/a$ and $q_c^{\rm II}=\pi/l_F$, respectively.

$c_1^*(\alpha)$ (line AB of Fig. 7), a localized region together with a pair of mobility edges appears (or disappears) on the lower-frequency side. As we cross the critical line $c_2^*(\alpha)$ (line AF of Fig. 7), an extended region together with a pair of mobility edge disappears (or appears) on the higher-frequency side. Also, on these boundaries, $\xi_{\rm cor}$ (or $\xi_{\rm loc}$) diverges at some isolated frequency from both sides with an exponent $\nu=2$. Point A is a critical point of higher order where three roots of $x(E)=1$ coincide at E^{***}. In this case, $\xi_{\rm cor}$ and $\xi_{\rm loc}$ diverge at E^{***}, respectively, from left and right sides with an exponent $\nu=3$.

Finally, we make some remarks on the reliability of our results. The CPA equations for the averaged one-phonon Green's function and the corresponding DOS were first given by Taylor.[27] Although the original forms are different from our Eqs. (8)–(10) and (15), it can be shown that they are equivalent. In three dimensions, Taylor has compared the CPA DOS which was calculated using a realistic unperturbed Green's function with the numerical simulation results of Payton and Visscher[28] for the case $\alpha=3$ and $c=0.240$, 0.491, 0.760, and 0.866 (Fig. 9 of Ref. 27). The CPA was shown to give very accurate results except in the high-frequency subband when $c=0.760$ and 0.866. This is the worst region of CPA, where the single-site theory can not reproduce the pronounced spikes of the machine results due to the localized modes from the clusters of the light mass atoms. Since we have used the semi-elliptical band approximation for the unperturbed Green's function, our CPA, DOS is different from that of Taylor. When $\alpha=3$, we have compared our DOS for the case of $c=0.5$ (Fig. 3) and 0.75 (Fig. 4) with the results of Taylor and simulation data at $c=0.491$ and 0.761, respectively. This is done by transforming our units to the units of Ref. 27, i.e., $z=E^2/12$ and $\nu'(z)=6\rho(E)/E$. Except the high-frequency subband of the case $c=0.75$, where we have a smooth DOS instead of spiky peaks, our DOS curves give the correct locations of the peaks, dip, gap, and band edges to within 10%. However, the heights of our DOS curves are a factor of 1.5 lower than the simulation data. This is due to the semi-elliptical band approximation we

have used in the unperturbed DOS which is known to give a lower height (also about a factor of 1.5) in comparison with the exact unperturbed DOS.[17] The main effect of the semi-elliptical band approximation is to introduce quantitative errors in DOS and diffusion constant. We think that the effect on the phase transition properties like $c_1^*(\alpha)$ and the corresponding critical frequency $E_1^{**}(\alpha)$ will be smaller. This is because the location of the dip in DOS which signals the resonance scattering frequency is more important in determining the occurrence of the localization transition. We believe that the major uncertainty in the phase diagram (Fig. 7) and the location of the mobility edges are caused by the arbitrariness in the cutoff q_c inherent to the theory. Nevertheless, even in the worst region of CPA DOS, where the light mass atoms do not percolate, $c > 1-p_c$ (the region above the *AF* line in Fig. 7), this theory can still predict correctly that all states in the high-frequency subband are localized.

ACKNOWLEDGMENTS

The authors wish to thank Z. B. Su and Ping Sheng for useful discussions. The work was supported by National Science Foundation of China.

[1]See, for example, P. A. Lee and T. V. Ramakrishnan, Rev. Mod. Phys. **57**, 339 (1985).
[2]E. Abrahams, P. W. Anderson, D. C. Licciardello, and T. V. Ramakrishnan, Phys. Rev. Lett. **42**, 673 (1979).
[3]A. D. Zdetsis, C. M. Soukoulis, E. N. Economou, and G. S. Grest, Phys. Rev. B **32**, 7811 (1985).
[4]B. Bulka, M. Schreiber, and B. Kramer, Z. Phys. B **66**, 21 (1987).
[5]E. Kolley and W. Kolley, Z. Phys. B **65**, 7 (1986).
[6]S. John, H. Sompolinsky, and M. J. Stephen, Phys. Rev. B **27**, 5592 (1983); S. John, *ibid.* **31**, 304 (1985).
[7]T. R. Kirkpatrick, Phys. Rev. B **31**, 5746 (1985).
[8]P. Shen and Z. Q. Zhang, Phys. Rev. Lett. **57**, 1879 (1986).
[9]K. Arya, Z. B. Su, and J. L. Birman, Phys. Rev. Lett. **54**, 1559 (1985); **57**, 2725 (1986).
[10]R. Bruinsma and S. N. Coppersmith, Phys. Rev. B **33**, 6541 (1986).
[11]M. L. William and H. J. Maris, Phys. Rev. B **31**, 4508 (1985).
[12]E. Akkermans and R. Maynard, Phys. Rev. B **32**, 7850 (1985).
[13]J. Canisius and J. L. van Hemmen, J. Phys. C **18**, 4873 (1985).
[14]S. He and J. D. Maynard, Phys. Rev. Lett. **57**, 3171 (1986).
[15]J. E. Graebner, B. Golding, and L. C. Allen, Phys. Rev. B **34**, 5696 (1986).
[16]D. Vollhardt and P. Wölfle, Phys. Rev. Lett. **45**, 842 (1980); Phys. Rev. B **22**, 4666 (1980).
[17]See, for example, E. N. Economou, *Green's Function in Quantum Physics*, 2nd ed. (Springer-Verlag, New York, 1983).
[18]B. Velicky, Phys. Rev. **184**, 614 (1969).
[19]R. J. Elliott, J. A. Krumhansl, and P. L. Leath, Rev. Mod. Phys. **46**, 465 (1974).
[20]R. J. Elliott and D. W. Taylor, Proc. R. Soc. London, Ser. A **296**, 161 (1967).
[21]T. Kopp, J. Phys. C **17**, 1919 (1984).
[22]A. B. Chen, G. Weisz, and A. Sher, Phys. Rev. B **5**, 2897 (1972).
[23]B. Velick, S. Kirkpatrick, and H. Ehrenreich, Phys. Rev. **175**, 741 (1968).
[24]J. Stein and U. Krey, Z. Phys. B **34**, 287 (1979); Physica **106A**, 326 (1981).
[25]S. Sarker and E. Domany, Phys. Rev. B **23**, 6018 (1981).
[26]Ora Entin-Wohlman, S. Alexander, R. Orbach, and Kin-wah Yu, Phys. Rev. B **29**, 458 (1984).
[27]D. W. Taylor, Phys. Rev. **156**, 1017 (1967).
[28]D. N. Payton and W. M. Visscher, Phys. Rev. **154**, 802 (1967).